Journal of Cell Science 108, 1519-1530 (1995)
Printed in Great Britain © The Company of Biologists Limited 1995



# Motility and substratum adhesion of *Dictyostelium* wild-type and cytoskeletal mutant cells: a study by RICM/bright-field double-view image analysis

**Igor Weber, Eva Wallraff, Richard Albrecht and Günther Gerisch***

Max-Planck-Institut für Biochemie, D-82152 Martinsried, Germany

*Author for correspondence

## SUMMARY

**To investigate the dynamics of cell-substratum adhesion during locomotion, a double-view optical technique and computer-assisted image analysis has been developed which combines reflection interference contrast microscopy (RICM) with bright-field imaging. The simultaneous recording of cell-substratum contact and cell body contour has been applied to aggregation-competent cells of *Dictyostelium discoideum*. These cells are distinguished from cells at earlier stages of development by small areas of contact to a substratum.**

**Three questions have been addressed in analysing the locomotion of aggregation-competent cells. (1) What is the relationship between changes in the shape of cells and their contact to a substratum during a chemotactic response? (2) What is the relationship between protrusion and retraction of the cell body, and between local attachment and detachment? (3) Are there differences between wild-type and mutant cells that lack certain cytoskeletal proteins?**

**During a chemotactic response the front region of the amoeba can bend towards the gradient of attractant without being supported by its contact with a surface, which excludes the necessity for gradients of adhesion for the response. The finding that in locomoting cells protrusion of the leading edge often precedes retraction establishes a pioneer role for the front region. The finding that gain of contact area precedes loss provides evidence for the coordination of interactions between the cell surface and a substratum. For comparison with wild-type, aggregation-competent triple mutant cells have been used that lack two F-actin crosslinking proteins, α-actinin and 120 kDa gelation factor, and an actin filament fragmenting protein, severin. Disturbances in the spatial and temporal control of cytoskeletal activities have been unravelled in the mutant by RICM and quantified by cross-correlation analysis of attachment and detachment vectors. In order to detect these disturbances, it was essential to analyse cell locomotion on the weakly adhesive surface of freshly cleaved mica.**

Key words: *Dictyostelium discoideum*, locomotion, cell-substratum adhesion, cytoskeleton, actin binding protein, reflection interference contrast, time series analysis, cross-correlation

## INTRODUCTION

The highly motile cells of *Dictyostelium discoideum* are useful models to study the dynamics of the actin-based cytoskeleton by a combination of biochemical studies, genetic manipulation, and quantitative analysis of cell locomotion and shape changes (for reviews, see Luna and Condeelis, 1990; Egelhoff and Spudich, 1991; Schleicher and Noegel, 1992; Condeelis, 1993; Gerisch et al., 1993). Motor proteins and accessory proteins of the actin cytoskeleton have been biochemically characterised and their function in vivo determined by the isolation of mutants (for the proteins relevant to this paper, see Wallraff et al., 1986; André et al., 1989; Brink et al., 1990; Cox et al., 1992; Witke et al., 1992). Optical microscopy combined with digital image processing have provided analytical tools to study motility of wild-type and mutant cells. These tools have been applied to quantify chemotactic responses of *Dictyostelium* cells (Fisher et al., 1989) and to describe the two- and three-dimensional organisation of locomoting cells (Soll, 1988; Killich et al., 1993; Wessels et al., 1994).

In *Dictyostelium* as in vertebrate cells, locomotion is determined by the spatio-temporal pattern of activities of the cytoskeleton and by the strength and dynamics of cell adhesion to a substratum. General concepts and techniques for the quantitative analysis of locomotion have been outlined by Dunn and Brown (1987) and Albrecht-Bühler (1990). Global information can be obtained by reducing cell motion to motion of the centroid of two-dimensional cell projections. Since this information can be obtained at low magnification, simultaneous tracking of many cells is possible. The paths of locomotion can be mathematically analysed and parameters of persistent or biased random walk extracted (Alt, 1990a; Stokes et al., 1991). It has become clear from these studies that cells have mechanisms at their disposal to control and stabilise their direction and speed of motion.

Tracking of centroids has also been employed to study the dependence of cell migration on receptor-mediated adhesion to a substratum (DiMilla et al., 1993). An optimal strength of adhesion has been found for cell locomotion, in accord with theoretical considerations predicting that locomotion is

inhibited if interaction with a substratum is too strong or too weak (Lauffenburger, 1989; DiMilla et al., 1991; Dickinson and Tranquillo, 1993).

In order to understand cell locomotion in terms of cytoskeletal dynamics and the forces generated by cytoskeleton-membrane coupling (Sackmann, 1994; Oliver et al., 1994), global methods of cell tracking have to be complemented by detailed studies at the single-cell level (Alt, 1990b; Simon and Schmidt-Schönbein, 1990; Lee et al., 1993). The method of choice for recording cell-to-substratum adhesion in locomoting cells is reflection interference contrast microscopy (RICM) (Curtis, 1964; Gingell and Todd, 1979; Versucheren, 1985; Rädler and Sackmann, 1993). This technique has been applied to *Dictyostelium* cells in order to investigate contact-induced changes of cell shape (Gingell and Vince, 1982; Owens et al., 1988). The power of combining RICM with digital image processing as a tool to analyse the dynamics of cell-to-substratum contacts has been demonstrated by Schindl et al. (1995). These authors have introduced freshly cleaved mica surfaces for the detection of subtle alterations in cell-to-substratum adhesion of *Dictyostelium* cells, and have found deficiencies in the control of locomotion that are associated with mutations in actin-binding proteins.

In order to relate information on the contact area to the shape of the cell body, we have developed a double-view video microscopy technique which combines RICM with bright-field microscopy (BFM). Using this technique we show in this paper that chemotactic orientation of a cell can be initiated by a shape change without support by cell-to-substratum adhesion. By time series analysis of RICM and BFM images, correlations have been unravelled between attachment at one site of the cell surface and detachment at another, and also between protrusion and retraction of the cell body during locomotion. In the course of this work, time series analysis has become an efficient method for the analysis of deficiencies in spatio-temporal coordination of local activities in mutant cells lacking actin-binding proteins.

## MATERIALS AND METHODS

### Strains and culture conditions

Cells of *D. discoideum* strain AX2-214, here referred to as wild-type, and the cytoskeletal triple mutant strain TP1 were used. Mutant TP1 lacks the two F-actin crosslinking proteins α-actinin and 120 kDa gelation factor as well as the actin filament fragmenting protein severin. The construction and genotype of the mutant have been described by Schindl et al. (1995). Cells were cultivated in liquid nutrient medium as described by Malchow et al. (1972), and harvested during exponential growth ($\leq 2\times10^6$ cells/ml for the mutant, $\leq 5\times10^6$ cells/ml for the wild-type). Washed cells were starved in 17 mM Sörensen K/Na phosphate buffer, pH 6.0 ('starvation buffer') at a density of $1\times10^7$ cells/ml and incubated at 150 rpm on a rotary shaker at 22-24°C. Aggregation-competent cells were harvested between 6 and 7 hours of starvation, when they had formed large clumps in suspension. A 1 ml sample of the suspension was centrifuged and cells were dissociated during resuspension in fresh starvation buffer by gently drawing them repeatedly through a plastic pipette tip. The cell density was reduced by two 1:100 steps of dilution in starvation buffer to $1\times10^3$ cells/ml. One droplet of cell suspension containing about 300 cells in 0.3 ml was deposited on the experimental surface, and experiments were initiated 10 minutes thereafter, when the cells had settled.

### Preparation of substrata and chemotactic stimulation

The experimental chamber consisted of a Plexiglas ring of 16 mm in diameter glued to a coverslip with silicon grease. Coverslips (40 mm × 24 mm) were cleaned by overnight immersion in 1 M HCl, followed by washes in double-distilled water and acetone. For experiments on BSA-coated glass, a solution of 0.2% BSA (bovine serum albumin, Serva, Heidelberg) was placed inside the ring for 10 minutes to allow the protein to adsorb, then washed three times with starvation buffer. To produce a strongly adhesive surface, coverslips were silanized by immersion for 10 seconds in a solution of 20 mg/ml of dimethyldichlorosilane in 1,1,1-trichloroethane (Pharmacia, Uppsala, Sweden) and subsequently washed in chloroform.

For experiments on mica, sheets of a few micrometers thickness were cleaved off from mica plates (Bio-Rad, Watford, UK) and optically coupled to coverslips by a thin layer of immersion oil. The Plexiglas ring was then attached to the mica surface using silicon grease. Splitting of mica layers occasionally led to boundaries between zones of different thickness. Only cells not crossing these borders were considered, thus excluding any guidance effects (Dunn and Brown, 1986).

Cells were chemotactically stimulated essentially as described by Gerisch and Keller (1981). Borosilicate glass micropipettes with an opening of about 0.4 μm were made on a Flaming/Brown micropipette puller (Model P97, Sutter Instruments Co., Novato, CA, USA). Micropipettes were filled with $1\times10^{-4}$ M cAMP solution and introduced into the experimental chamber using a Leitz mechanical micromanipulator.

### Double-view microscopy

The experimental set-up consisted of an Axiovert 135 microscope (Carl Zeiss, Oberkochen) equipped with two video exits separated by an FT 580 dichroic mirror (Fig. 1). For RICM imaging, the epifluorescence optical path of the microscope was used (for principles of RICM, see Rädler and Sackmann, 1993). The 546 nm line of a 100 W mercury lamp was selected by an IF 546 interference filter (Zeiss). An 64 Antiflex objective equipped with a λ/4 plate was used and the illuminating numerical aperture adjusted to 0.9.

For simultaneous BFM and RICM imaging, 600-700 nm light was isolated by combining a high-pass glass filter, cut-on 600 nm, with a heat-protecting filter (Zeiss). An LD 0.55 H long-distance condenser (Zeiss) was used for illumination. The transmitted and reflected light beams were separated by the dichroic mirror ($\lambda_{sep}$=580 nm). Since the reflected light accounted only for a small percentage of the total light intensity, disturbing red light was filtered out of the RICM optical path using a BP 515-565 band-pass filter (Zeiss).

### Image acquisition and processing

RICM and BFM images were obtained using two identical VS450 CCD cameras (Stemmer, 82178 Puchheim, Germany). The cameras were aligned with each other by bringing images of a rectangular grid into coincidence (Galbraith and Farkas, 1993), resulting in precision of ±1 pixel in both directions. The images were digitised in 256 grey levels using an OFG digitising board (Imaging Technology Inc., Woburn, MA, USA). Since this board supports multiple camera inputs, the two images could be transferred into the board's memory almost simultaneously, the interval between images being less than 0.1 second. Grey-level images of 384×384 pixels, corresponding to 47×47 μm in the plane of the object, were stored on a hard disk for further processing. In order to monitor cells that leave the field, we used a step motor-driven, computer-controlled scanning table (MK32, Märzhäuser, 35579 Wetzlar, Germany). Image acquisition was controlled during an experiment through an IBM-compatible PC 486/50 by an interactive program written in C programming language. This program allowed on-line control of the OFG board functions: cameras, image sizes, table movements over a control unit (Multi Control 2000, Märzhäuser), focusing control, and timing. Each cell

was monitored for 10 minutes, with intervals of 5 seconds between each pair of images.

Contact areas of cells were extracted from RICM images by a routine which performs binarisation on the basis of threshold estimation, as it is calculated by a histogram minimum method (Russ, 1990). A lower size limit for a segment of a contact area was set to 1 $\mu m^2$. With one step of median filtering, the algorithm required about 4 seconds per image, and proved to be stable irrespective of noise, changes in contrast quality and illumination. Boundaries of cells were extracted from bright-field images by means of an algorithm that included background subtraction and binarisation based on texture discrimination by means of a rank operator. Since this procedure involved extensive serial convolutions and iterative steps, it took about 50 seconds to analyse an image. Both the RICM and BFM extracting routines were written in the form of menu-driven programs using only compiler-supplied functions (HighC, Metaware, Santa Cruz, CA, USA). Binarised images were analysed by the use of standard binary-editing tools, and the resulting data stored as an ASCII file.

### Definition of parameters

Gained and lost areas of cell body projections and of cell contacts to a substratum were determined from the binarised images. We define gained area ($G$) as all pixels that belong to an area in a given image but not in the preceding one. Lost area ($L$) is accordingly defined as all pixels that do not belong to an area in a given image but belonged to that area in the preceding image. Area that is not changed between two images is designated as constant area ($C$). We use symbols $G_b$, $L_b$ and $C_b$ for scalar parameters of cell body projections obtained by BFM, and $G_c$, $L_c$ and $C_c$ for scalar parameters of contact areas obtained by RICM. Two-dimensional vectors **P** and **R** for cell body protrusion and retraction, and **A** and **D** for attachments to, and detachments from, a substratum are defined as explained in Fig. 2.

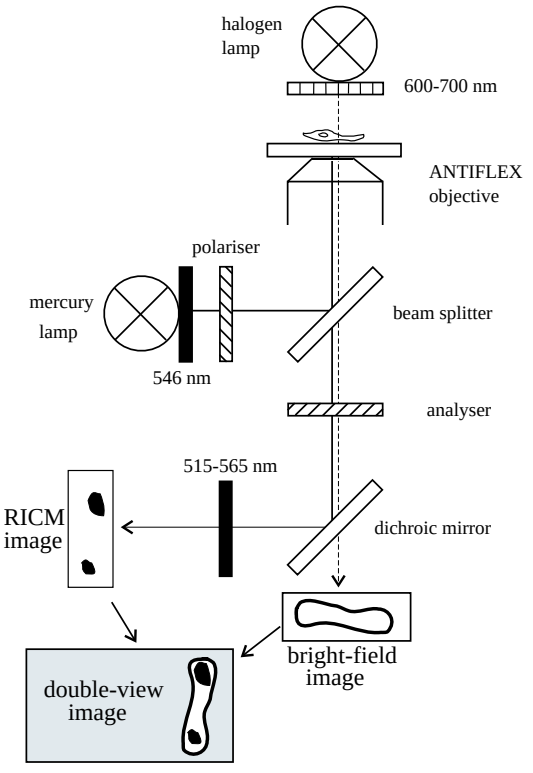


**Fig. 1.** Optical configuration used for double-view microscopy. The continuous line represents the green light which is reflected from the cell (RICM imaging), the broken line represents the transmitted red light (BFM imaging). Filters are indicated by the respective pass-bands (for broad-band filters) or central wavelength (for narrow-band filter). See text for details.

### Time series analysis

Sample cross-correlation coefficients for parallel time series of two scalar variables $G(i\tau)$ and $L(i\tau)$ ($i$=1,2...,$n$) are given at discrete time lags ($k\tau$, $k$ = 0, ±1, ±2,...) as:

$$r_k = c_k/c_0, \text{ where } c_k = \frac{1}{n-|k|}\sum_{i=1}^{n-k}(G_i-\bar{G})(L_{i+k}-\bar{L})$$

for $k\geq 0$, and

$$c_k = \frac{1}{n-|k|}\sum_{i=1-k}^{n}(G_i-\bar{G})(L_{i+k}-\bar{L})$$

for $k<0$.

The time interval between images, $\tau$, was 5 seconds in all experiments. $\bar{G}$ and $\bar{L}$ designate average values of each time series. In the case of vectors, we sum the scalar (dot) products between time-lagged vectors (Dunn and Brown, 1987) weighted by the sizes of corresponding areas. For two vector variables $\mathbf{X}(i\tau)$ and $\mathbf{Y}(i\tau)$, $c_k$ is defined as:

$$c_k = \frac{1}{n-|k|}\sum_{i=1}^{n-k}[(G_i-\bar{G})\mathbf{X}_i\cdot(L_{i+k}-\bar{L})\mathbf{Y}_{i+k}]$$

for $k\geq 0$, and

$$c_k = \frac{1}{n-|k|}\sum_{i=1-k}^{n}[(G_i-\bar{G})\mathbf{X}_i\cdot(L_{i+k}-\bar{L})\mathbf{Y}_{i+k}]$$

for $k<0$.

The length of the time series was always 10 minutes. Pooled cross-correlograms shown in Fig. 8 were obtained by summing values of cross-correlation coefficients for each time lag from all cells and dividing the sum by the number of cells. For simplicity, pooled cross-correlograms are further designated as $\langle G_bL_b\rangle$, $\langle G_cL_c\rangle$, $\langle \mathbf{P}\cdot\mathbf{R}\rangle$, and $\langle \mathbf{A}\cdot\mathbf{D}\rangle$, and time lags as $\delta t$.

### Statistical analysis of locomotion paths

For determining the locomotion paths shown in Fig. 5 and for their statistical analysis, the positions of centroids of cell body projections and the displacement vectors were defined according to Dunn and Brown (1987). We analysed paths of cell locomotion by fitting a plot

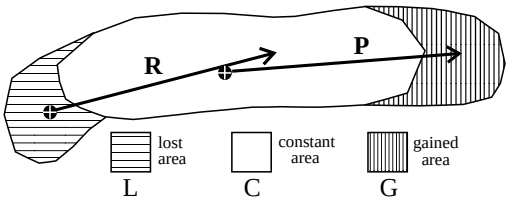


**Fig. 2.** Definition of the vectors of protrusion (**P**) and retraction (**R**). **P** points from the centroid of the cell contour in the preceding frame ($C$+$L$) towards the centroid of gained area ($G$). **R** points from the centroid of lost area ($L$) towards the centroid of the present cell contour ($C$+$G$). The vectors of attachment (**A**) and detachment (**D**) are defined in analogy to **P** and **R**, the only difference being that cell contour is replaced by contour of the contact area. In calculations, vectors are weighted by the sizes of gained or lost areas. Thus, modules of the vectors are proportional to the sizes of gained or lost areas and to their distances from the centre of cell contour.

of mean-square-displacements $<d^2>$ versus time to a persistent random walk model, to obtain root-mean-square speeds, *S*, and persistence times, *P* (Dunn, 1983; DiMilla et al., 1991). Results were averaged over all cells for each combination of the two strains and the two surfaces, and distributions compared by the non-parametric Mann-Whitney U-test.

## RESULTS

### Changes in cell shape and contact area at onset of the aggregation phase

During the growth phase and early development, cells of *D. discoideum* are extensively spread over a surface on which they move. They extend broad lamellipodia similar in shape to those of fibroblasts or keratinocytes (Fig. 3A). Sometimes the cells form ruffling edges all around their circumference without exhibiting any substantial net locomotion (Fig. 3B). After 6-7 hours of starvation under our conditions, cells become aggregation-competent, i.e. they acquire the capacity of assembling into streams and of responding chemotactically to cAMP. The acquisition of aggregation-competence is accompanied by distinct changes in cell shape and locomotion. Cells become elongated, they move with a sharply circumscribed front (Fig. 3C), and only transiently form multiple fronts that compete with each other (Fig. 3D).

As illustrated in Fig. 3, these shape changes are accompanied by a dramatic reduction in size of the area of contact between cell and substratum. In order to quantify this reduction, the contact areas ($A_c$) of one hundred randomly chosen growth-phase and aggregation-competent AX2 cells on BSA-coated glass were measured. Mean values and standard deviations were $A_c = 92 \pm 50\ \mu m^2$ for growth-phase and $A_c = 18 \pm 11\ \mu m^2$ for aggregation-competent cells. The small contact areas of aggregation-competent cells were often segmented, which means that the cells touched the surface at several separate sites of adhesion.

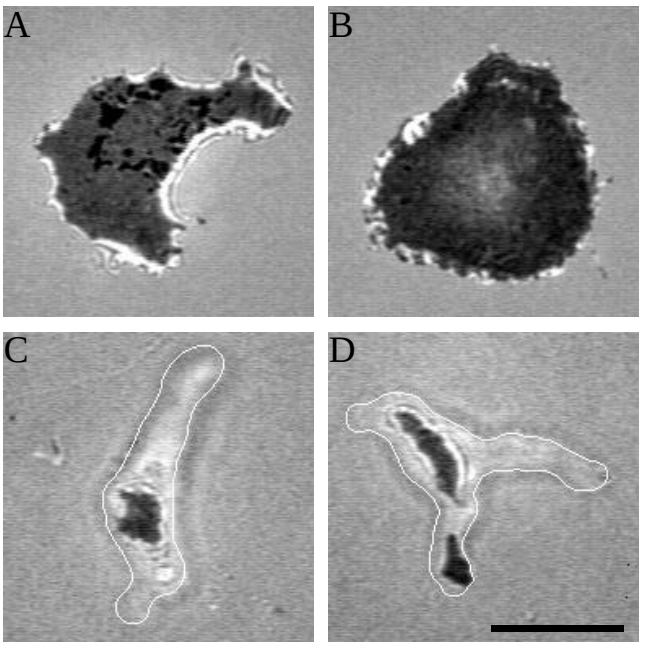


**Fig. 3.** RICM images of two growth-phase cells (A,B) and two aggregation-competent cells (C,D) of wild-type strain AX2 on BSA-coated glass. The darkest spots in (A) represent the vesiculotubular osmoregulatory apparatus on the ventral side of the cell (Gingell et al., 1982). The cell in B displays ruffling or lamellipodia all around its edge. The cell contours indicated in C and D by white lines show the elongated shape of developed cells. These contours have been obtained from bright-field images. The branched cell in D represents a transition state with the coexistence of two fronts. Bar, 10 μm.

Similar results to those found on the moderately adhesive BSA-coated glass surfaces were obtained on the weakly adhesive surfaces of freshly cleaved mica. On strongly adhesive silanized glass, aggregation-competent cells were in contact with the substratum over almost their entire ventral side and, accordingly, became more flattened. During locomotion, they left portions of their membrane behind in the form of small patches, as has been described for the movement of pre-aggregative cells on a strongly adhesive surface (Schindl et al., 1995). These results show that strong cell-to-substratum adhesion counteracts the changes in cell shape that typically occur during early development of *D. discoideum*.

### Relationship between changes in cell shape and contact area during chemotactic turning

When aggregation-competent cells are stimulated by cAMP that diffuses out of the tip of a micropipette, they respond either by turning with their established front into the gradient of attractant, or by protruding one or several new pseudopods towards the micropipette while redrawing from the previous front (Gerisch et al., 1975). The relationship between changes of cell shape and contact area during these responses was determined by the double-view microscope technique.

Chemotactic turning of a cell occurred either with the front region not in contact with a surface (Fig. 4A, 14-17), or with the front region spreading along a surface during its extension (Fig. 4B, 5-6). Likewise, new pseudopods induced by the attractant grew in length when they were extended into the free fluid space and also when they stayed in contact with a surface. The example of two competing pseudopods shown in Fig. 4A, frames 5-12, is of interest because a pseudopod that initially had not been in contact with the substratum finally became the persisting one.

### Cell locomotion in wild-type and in a cytoskeletal mutant on surfaces of different adhesiveness

In the following sections we concentrate on changes in cell shape and contact area that occur during unbiased locomotion of aggregation-competent cells, i.e. in the absence of chemotactic stimuli. Previous work on pre-aggregative cells has emphasised the fact that phenotypic changes associated with the lack of actin-binding proteins in *Dictyostelium* cells are most obvious on the weakly adhesive surfaces of freshly cleaved mica (Schindl et al., 1995).

Fig. 5 compares the locomotion behaviour of aggregation-competent wild-type cells and TP1 mutant cells that lack two F-actin crosslinking proteins, α-actinin and the 120 kDa gelation factor (ABP120), and also the F-actin fragmenting protein severin. These three proteins are characterised by potent activities in vitro (Brown et al., 1982; Condeelis et al., 1984; Eichinger and Schleicher, 1992; Witke et al., 1993). Mutations responsible for the lack of these proteins have been combined to produce a triple mutant for testing the functional conse-

quences of multiple defects in the cytoskeleton. Two parameters of cell locomotion, speed and persistence time of direction, were not distinguishable for wild-type cells moving either on BSA or on mica. These parameters were also similar for wild-type and mutant cells moving on BSA, but their values were significantly reduced for TP1 cells moving on mica (Fig. 5).

Figs 6 and 7 illustrate details of cell locomotion in relation to contact formation in wild-type and mutant TP1 cells. The protrusions of wild-type cells can grow into long extensions, independently of whether or not they attach to a substratum (Fig. 6A, frames 4 to 10, and Fig. 6B, frames 1 to 10). The same is true for mutant cells on BSA-coated glass. Fig. 7A, frames 2-6, show turning for a non-attached extension, which is reminiscent of changes in cell shape during a chemotactic response (Fig. 4). This behaviour has two implications. One is that new pseudopods can successfully compete with established ones even if they are not attached (Fig. 7A, frames 9-12). The other implication is that a cell can glide over almost stationary areas of contact (Fig. 6B, frames 2 to 10).

Gains of contact area are temporally related to losses of contact area; most often the gain precedes the loss. This holds for gain that is produced by attachment of the cell surface at a second separate site, so that the cell body bridges two areas of contact (Fig. 6A, frames 1 and 2), and also for gain produced by the extension of a continuous area of contact (Fig. 6A, frames 7 to 9) or by the fusion of two contact areas (Fig. 7A, frames 8 to 12).

Aberrations in mutant TP1 cells on mica are shown in Fig. 7B. On the weakly adhesive surfaces, mutant cells tend to be less elongated than wild-type cells. Portions of the cell body are protruded and retracted at short time intervals in different directions, and also fluctuations in the contact area appear over a smaller time scale.

### Principle of analysing protrusion-retraction and attachment-detachment dynamics in locomoting cells

In order to describe quantitatively the process of cell locomotion, the interplay of protrusion and retraction of the cell body on the one hand, and local attachment and detachment on the other, were analysed. Scalar values of gains and losses provide information on the extent of these processes, and vector variables contain information on their direction. The basic tool to uncover temporal relationships between these variables is the construction of cross-correlograms from time series. Variables are evaluated at discrete time intervals, in our case 5 seconds, and are correlated with each other at time lags corresponding to this interval and multiples thereof.

We define time lags so that their positive values designate relative precedence (lead in phase) of either protrusion or attachment. Cross-correlograms of scalar values of gains and losses $\langle GL \rangle$ are constructed from RICM images for the contact areas ($\langle G_c L_c \rangle$), and from bright-field images for two-dimensional projections of the cell body ($\langle G_b L_b \rangle$). Cross-correlograms of vectors ($\langle \mathbf{X} \cdot \mathbf{Y} \rangle$) are calculated for weighted vectors of attachment and detachment ($\langle \mathbf{A} \cdot \mathbf{D} \rangle$) from the spatial relationship of gains and losses of contact area, and for weighted vectors of protrusion and retraction ($\langle \mathbf{P} \cdot \mathbf{R} \rangle$) from the relationship of gains and losses of cell contour area (see Fig. 2). Since the correlation coefficients are, by definition, insensitive to variations in cell size, we can pool data from several cells and thus improve reliability of the correlation analysis.

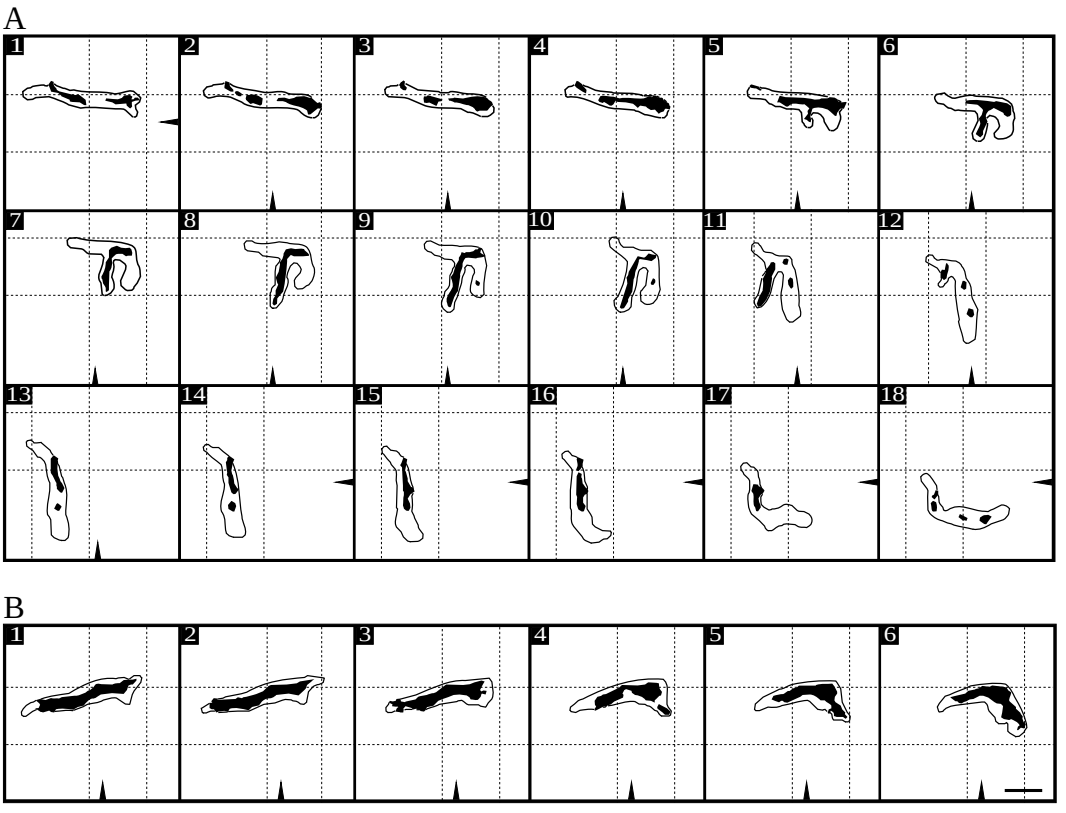


**Fig. 4.** Chemotactic turning of two wild-type AX2 cells (A and B) on BSA-coated glass, in response to steep attractant gradients produced by diffusion of cAMP out of the tip of a micropipette. Position of the tip is indicated in each frame. In A the position has been changed twice. Horizontal and vertical broken lines define a reference frame stationary with respect to the substratum. This frame accounts for translations of the microscope table. Interval between images, 10 seconds. Bar, 10 μm.

### Cross-correlograms of gains and losses of contact and cell contour areas

Time series analyses are summarised in Fig. 8. The locomotive behaviour of the cells was studied on BSA-coated glass and on mica as for Fig. 5. We discuss first the correlograms of the scalars $<G_cL_c>$ that refer to gains and losses of the contact area of wild-type AX2 cells (Fig. 8A and C). The most important feature of these correlograms is their asymmetry about $\delta t = 0$. Cross-correlation coefficients are significantly positive for time lags between 0 and +50 seconds, and become abruptly insignificant for negative $\delta t$ values. These data indicate that during locomotion, contact of the cells to the substratum fluctuates in a way that gain of area precedes loss of area. Loss follows the gain within 50 seconds; most often it occurs at 5 to 10 seconds after the gain. A feature of $<G_cL_c>$ only obvious on BSA coated glass, is a cluster of negative correlation coefficients between $\delta t = -80$ and $\delta t = -110$ seconds. Our interpretation of this cluster is that large detachments are followed by small attachments after about one and a half minutes (or small detachments followed by large attachments). These data point to a 'memory' that is implemented in the processes that control the interaction of cells with a substratum.

The correlograms for protrusion and retraction of the entire locomoting cell, $<G_bL_b>$, differ from those for attachment and detachment in being less distinctively asymmetric (Fig. 8E and G). The highest correlation is found at $\delta t = 0$, which means that retraction often occurs simultaneously with protrusion. Nevertheless, the correlation coefficients are higher at positive time lags than at negative ones. These data indicate that in a considerable number of cases retraction lags up to 15 seconds behind protrusion. In fewer cases retraction precedes protrusion for up to 15 seconds.

For mutant TP1, the overall shape of the correlograms of scalars, $<G_cL_c>$ and $<G_bL_b>$, is similar to that of wild-type, but there are some differences, the most relevant one being $<G_bL_b>$. As shown in Fig. 8M and O, the range of significant correlation coefficients is less extended than in wild-type (Fig. 8E and G). Also, the peak at $\delta t = 0$ is less prominent in the mutant. These data imply that protrusion and retraction are less tightly coupled to each other in the mutant than they are in the wild-type. In $<G_bL_b>$ on mica (Fig. 8O), a small group of negative correlation coefficients is seen around $\delta t = +60$ seconds, which might be due to a negative feedback implemented in the control system of cell motility. On BSA there are fluctuations in the correlation coefficients at $\delta t > 30$ seconds which might indicate oscillations, but are at the limit of significance. Finally, in mutant TP1 the cluster of negative correlation coefficients for $<G_cL_c>$ appears to be shifted to smaller negative time lags. The negative peak is at $\delta t = -95$ seconds in the wild-type (Fig. 8A) and at $\delta t = -75$ seconds in the mutant (I). This result may indicate an alteration in the 'memory' responsible for the control of cytoskeletal activities in the minute range.

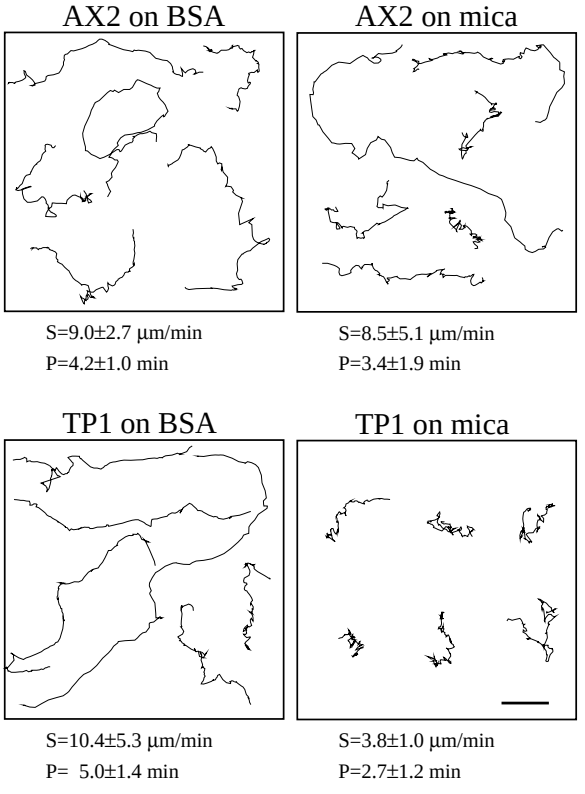


**Fig. 5.** Paths of wild-type AX2 and mutant TP1 cells moving on BSA-coated glass or on mica. For each panel 6 cells were randomly chosen. Displacements of centroids are based on cell contours from bright-field images. Average speeds (*S*) and persistence times (*P*) are indicated with standard deviations underneath each frame. Bar, 20 μm.

### Cross-correlograms of protrusion-retraction and attachment-detachment vectors

For attachment and detachment vectors of wild-type cells on BSA-coated glass or mica (Fig. 8B and D), the correlograms show positive correlation coefficients with a similar asymmetry around $\delta t = 0$, as the correlograms for scalars (Fig. 8A and C). The interpretation of this result is that detachment goes with high probability in a direction similar to the direction that attachment has gone 5 to 15 seconds before. The results for vectors of protrusion and retraction of the cell body are different (Fig. 8F and H). Correlation coefficients of these vectors are significantly positive only at $\delta t = 0$. This means, at a given time the cells protrude and retract with significant probability in the same direction.

The correlograms for mutant TP1 cells on BSA-coated glass are similar to those of wild-type cells (Fig. 8J and N). However, on mica the most relevant alteration is seen in the correlograms of attachment-detachment and protrusion-retraction vectors (Fig. 8L and P). In both cases correlation coefficients are changed in sign relative to wild-type cells and also relative to mutant cells on BSA. The negative coefficients are asymmetrically distributed, as for the corresponding scalar values (Fig. 8K and O). Together with the positive values for scalars, the data in Fig. 8L and P show that vectors tend to point into opposite directions. This means that for the mutant cells on mica events of attachment and detachment that follow shortly after each other are likely to have opposite directions, and that the same is true for protrusion and retraction of the cell body. These data reflect the behaviour of mutant cells seen in Fig. 7B, where protruded pseudopods tend to be retracted after a short period of time.

## DISCUSSION

### Switch in cell locomotion and attachment during early development

The combination of bright-field imaging with reflection interference contrast microscopy (RICM) in the double-view system introduced in this paper proved to be a powerful tool to analyse the relationships between changes in cell shape and contact area during locomotion. Application of this system to the amoeboid cells of *D. discoideum* revealed dramatic changes during early development in the interaction of cells with a substratum that are correlated with changes in cell shape (Fig. 3).

The differences between growth-phase and aggregating cells of *D. discoideum* resemble differences between a variety of cells from other organisms. As pointed out by Harris (1994), distinct types of motility behaviour are paralleled by specific shapes of the cells. Fibroblasts and keratinocytes, on the one hand, are characterised by flat ruffling lamellipodia and by large areas of contact with a substratum that extend over almost their entire ventral surface. Large freshwater amoebae like *Amoeba proteus* or *Chaos carolinensis*, on the other hand, move with cylindrical pseudopods and touch their substratum only at a few points (Grebecki, 1994).

Cells of *D. discoideum* switch within about 6 hours from a fibroblast-like to an *A. proteus* type of behaviour. This switch might be due to the expression of new cytoskeletal proteins during the pre-aggregation phase or to changes in the activity of pre-existing proteins. A number of actin-binding proteins from *D. discoideum* are known to be regulated by phosphorylation or by the binding of ligands, for instance $PIP_2$ or $Ca^{2+}$ (for review, see Janmey, 1994). Whatever the mechanisms are, the changes in shape and adhesion of cells to a substratum during the early stages of development indicate that extreme differences in the behaviour of locomoting cells can be obtained by modifications in basically the same set-up of cytoskeletal components.

### Chemotaxis in *D. discoideum* cells as a shape change

Because of the switch in locomotory behaviour and attachment during the pre-aggregation phase, reproducible results are obtained in *D. discoideum* only with cells of a defined developmental stage. The fully aggregation-competent cells used in this paper have the appealing feature that their motion is directed within seconds towards externally applied cAMP. Because attachment to a substratum is often restricted to small surface areas in these cells, they are optimally suited to explore whether control of cell-to-substratum adhesion by a chemoattractant is an essential factor in reorientation. The data obtained demonstrate that the chemotactic response is, in principle, a bending reaction which does not need to be supported by adhesiveness (Fig. 4). During turning of a cell new pseudopods protruded either in contact with, or separate from a substratum, and in the case of competing pseudopods it was not (or not only) the attachment to a surface that decided between their persistence or retraction (Figs 4 and 6A). It should be pointed out here that the shape of wild-type cells of *D. discoideum* is less dependent on attachment to a substratum than the shape of fibroblasts. *D. discoideum* cells keep their amoeboid shape in suspension and, in the aggregation-competent stage, they can elongate by their own forces without any anchorage to a surface.

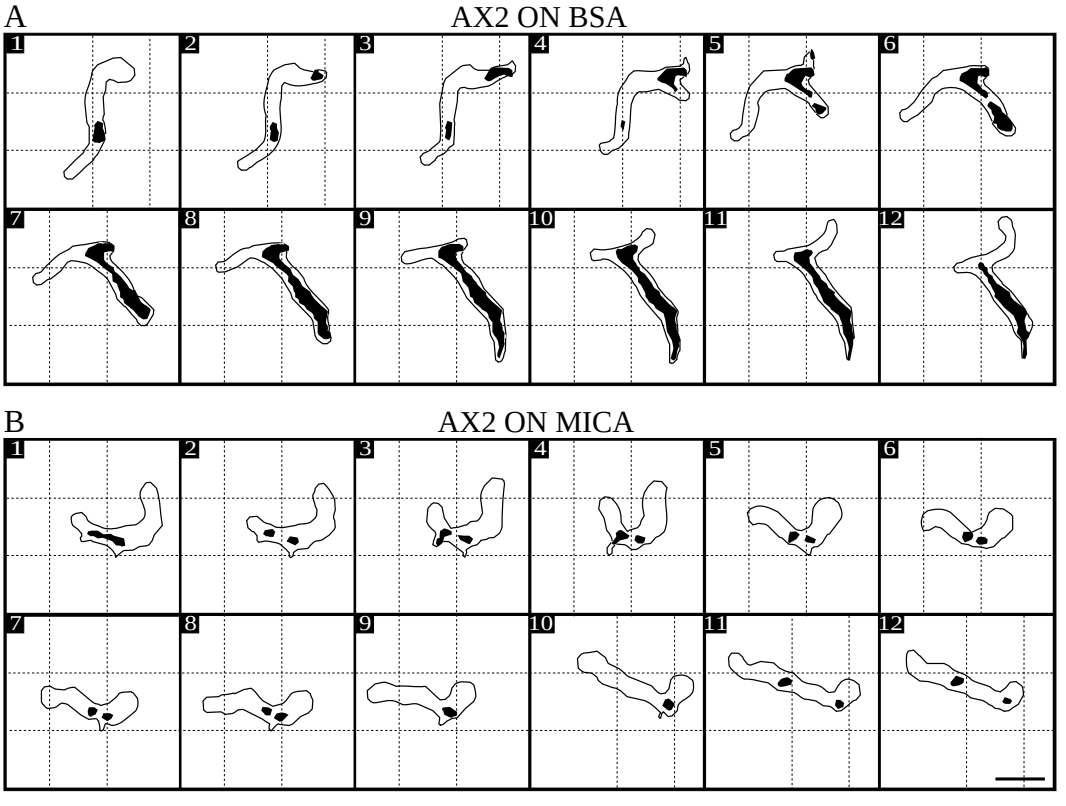


**Fig. 6.** Sequences illustrating characteristic features of motility in wild-type AX2 cells on BSA-coated glass (A) and mica (B). Horizontal and vertical broken lines define a reference frame which is stationary with respect to the substratum. Interval between images, 5 seconds. Bar, 10 μm.

### Coupling between protrusion and retraction, and coordination between cell attachment and detachment

The persistence of direction during locomotion of amoeboid cells requires the coordination in time and space of local activities within the actin cortex. Protrusion and retraction need to be coordinated, and the temporal and spatial pattern of attachment and detachment is also important for the crawling of a cell on a surface. One way to determine how all the local activities in a locomoting cell are coordinated is to compare wild-type and mutant cells with defined cytoskeletal defects by time series analysis. Here we discuss first the results obtained with wild-type cells. A principal finding is that cross-correlograms of scalars for the gain and loss of contact area are more strongly asymmetric than the cross-correlograms for protrusion and retraction of the cell body (Fig. 8A and C versus E and G). The conclusion from these results is that a cell makes and disrupts contacts with a substratum in a distinctly stepwise mode. The loss of contact area is coupled to gain; the gain almost always precedes the loss. The cross-correlograms of vectors indicate a high probability for detachment to occur in the same direction as the preceding attachment (Fig. 8B and D).

The cross-correlograms for protrusion versus retraction of the cell body remarkably differ from those of attachment versus detachment by a peak at zero time lag. This peak indicates a high propensity for expansion and contraction to occur simultaneously and in the same direction (Fig. 8E and G, F and H). Nevertheless, cross-correlograms of the scalars shown in Fig. 8E and G, have a bias for positive coefficients at positive time lags. This means that protrusion more often precedes than follows retraction.

### Appropriate adhesion to a substratum partly compensates for cytoskeletal defects

Mutant TP1 is defective in three actin-binding proteins, two of them exhibiting high actin-crosslinking activity in vitro. In a previous paper, pre-aggregative cells of this mutant have been shown by RICM to differ from wild-type cells by smaller areas of contact on the weakly adhesive surfaces of freshly cleaved mica, and by a reduced stability of pseudopods protruded along the mica surfaces (Schindl et al., 1995).

In the aggregation-competent stage that we have studied, wild-type cells formed even smaller areas of contact than the pre-aggregative mutant cells. Nevertheless, the aggregation-competent wild-type cells proved to be capable of stabilising the direction of their locomotion on mica as they do on more strongly adhesive surfaces, indicating that the mode of locomotion is not only determined by the size of the contact area but also by characteristics of cell organisation that are inherent to a given developmental stage. Locomotion in the aggregation-competent stage is best illustrated by the smooth gliding of a cell over an area of contact that remains nearly fixed relative to the substratum until the cell attaches at a new site (Fig. 6B).

Paths of locomotion with short persistence times of direction are typical of TP1 mutant cells crawling on mica (Fig. 5). On these weakly adhesive surfaces the extension of pseudopods is often immediately followed by their retraction, which leads to a reversal in the direction of movement (Fig. 7B). In the cross-correlograms of vectors, the destabilisation of locomotion in TP1 cells is reflected in the negative correlation coefficients obtained for protrusion and retraction, and also for attachment and detachment (Fig. 8L and P).

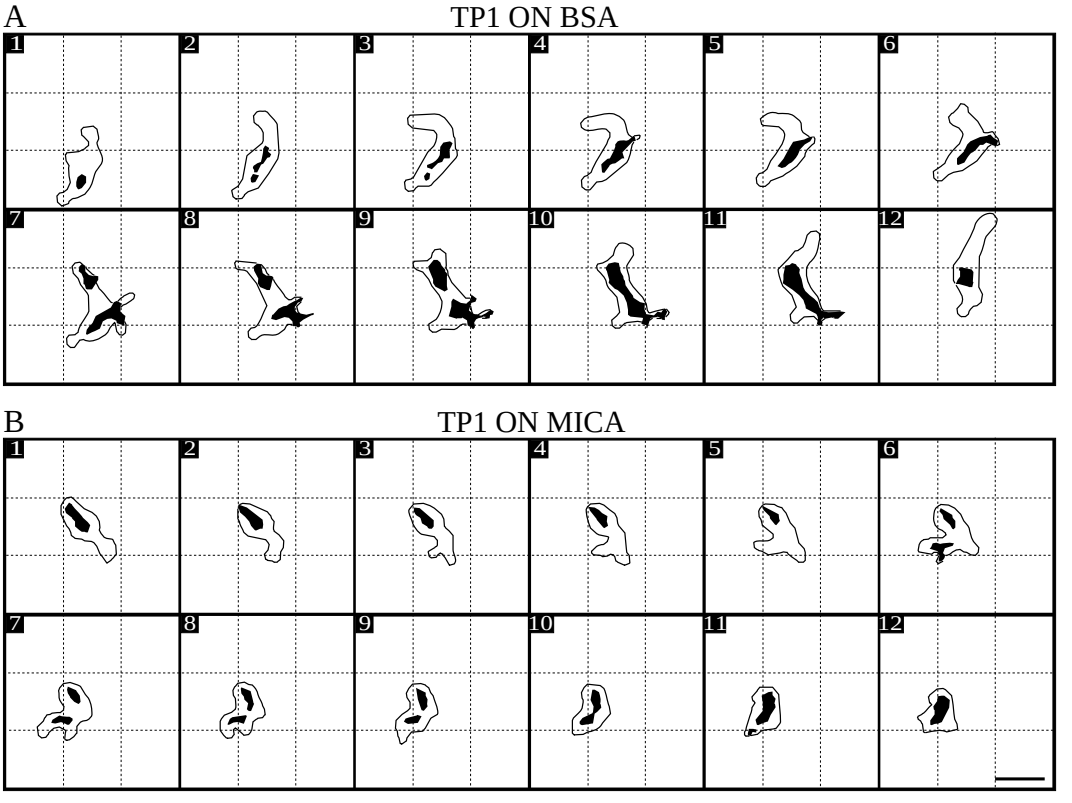


**Fig. 7.** Sequences illustrating locomotion of triple mutant TP1 cells on BSA-coated glass (A) or mica (B). Horizontal and vertical broken lines define a reference frame as in Fig. 6. Interval between images, 5 seconds. Bar, 10 μm.

In TP1 cells retraction of the cell body is inefficiently coupled to protrusion, as deduced from the strongly asymmetric cross-correlograms of scalars for protrusion versus retraction. This asymmetry is most distinct for cells on mica (Fig. 8O compared to G and M), but is also recognised on BSA-coated glass by the absence of a prominent peak at zero time lag (Fig. 8M compared to E). These data indicate a net gain of area covered by the cell-body projections (that we have used to measure protrusion and retraction) during the extension of pseudopods. Since the volume of a cell is assumed to be practically constant during locomotion, the fraction of the cell volume required for protrusion must be compensated in the mutant by a decrease in thickness of the TP1 cell. This behaviour resembles that previously described for the AX4 strain of *D. discoideum* (Wessels et al., 1994).

Only minor aberrations are seen in aggregation-competent cells of the TP1 mutant moving on BSA-coated glass, a substratum that is more adhesive than mica. This finding implies that the cytoskeletal proteins missing in the mutant, although they contribute to the mechanical properties of the actin network, have no substantial influence under optimal conditions. In particular, appropriate adhesion to a substratum can compensate for the lack of these proteins. Two reservations have to be added to this statement. First, the statement applies only to cells in which other actin-binding proteins sufficiently stabilise the actin cortex in the absence of the three actin-binding proteins missing in TP1 cells. This means the phenotype of mutants depends on their genetic background, which may differ in various laboratory strains referred to as wild-type. Second, the statement applies only to single-cell

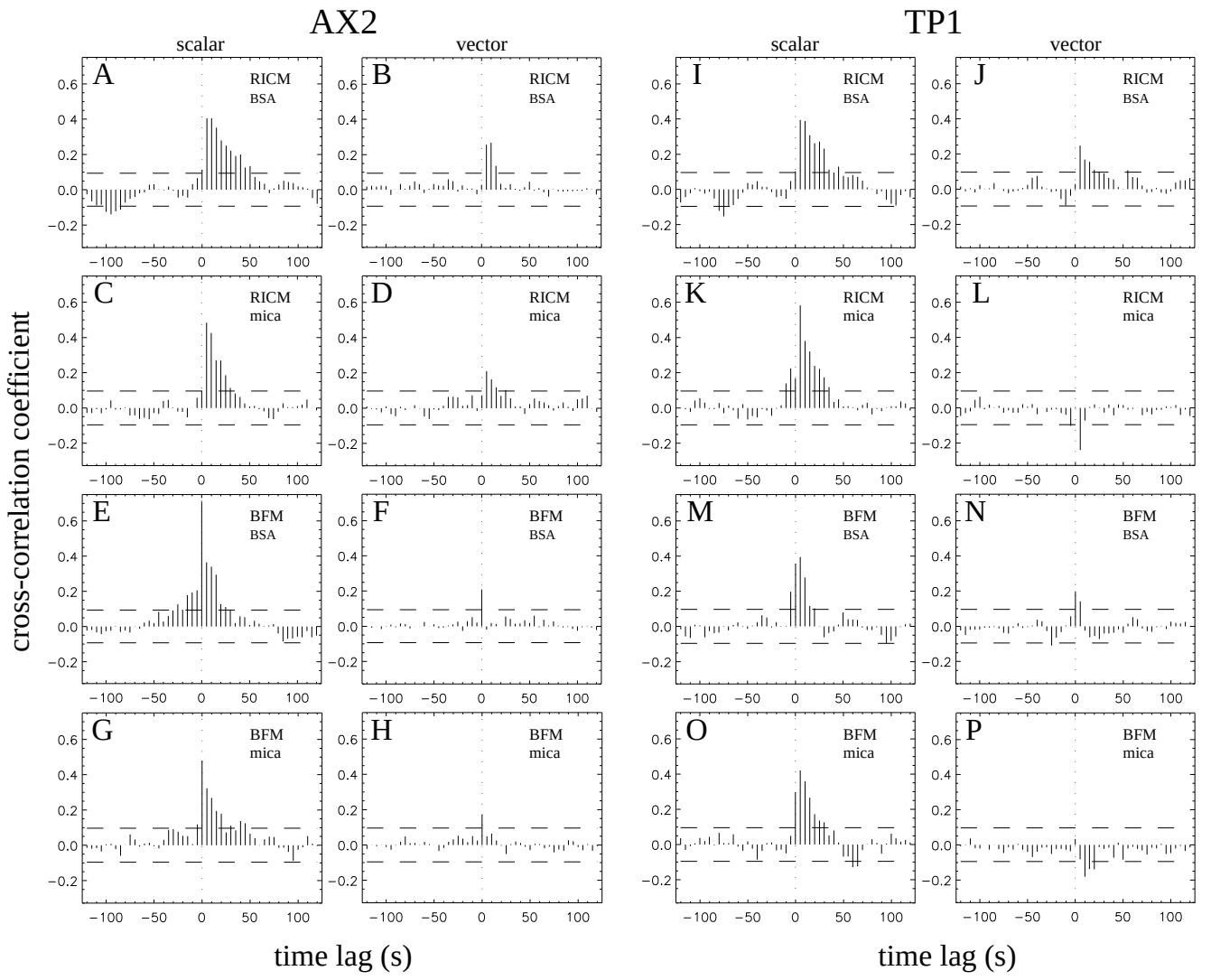


**Fig. 8.** Cross-correlograms for changes in cell body projection and contact area of locomoting cells. Left panels: cross-correlograms between lost and gained areas from RICM and BFM images of aggregation-competent wild-type AX2 cells. Right panels: the same for cells of mutant TP1 defective in three actin-binding proteins. Plots for scalar and vector parameters are aligned side-by-side in adjacent columns. Type of imaging (RICM for contact area and BFM for cell contour) and substratum (BSA or mica) are designated in each panel. For instance, J shows the correlogram <**A**·**D**> between attachment and detachment vectors of TP1 cells on bovine serum albumin. Correlograms are pooled from six cells, each monitored for a period of 10 minutes. Images have been taken every 5 seconds. Values for time lags from 0 to ±2 minutes are shown. Horizontal broken lines represent 99% significance limits. Vertical dotted lines mark the $\delta t$=0 position.

behaviour. Multicellular development is severely impaired in α-actinin/120 kDa double crosslinker mutants (Witke et al., 1992).

### The significance of cross-correlation data to models of cell locomotion

According to certain models, processes at a leading edge are initiated independently of activities at the rear; according to other models, protrusion of a front is brought about by contraction at the tail. Our finding that protrusion more often precedes than follows retraction is in accord with models of the first category. In these models protrusion is attributed to forces caused by an increase in length of actin-filament bundles (Condeelis, 1993) or to forces generated through forward propelling of actin filaments by membrane-anchored motor proteins of the myosin I type (Pollard et al., 1991; Sheetz et al., 1992; Titus, 1993). Our results do not distinguish between these possibilities. A model of the second category, proposing evagination at the front of a cell is caused by internal pressure that is generated at the rear, can be excluded. However, because of the temporal overlap of events at the front and the rear, the possibility is not excluded that a contracting tail feeds back to the front to allow its continued protrusion.

The disturbed coupling between front and rear events in the cytoskeletal mutant TP1 suggests that integrity of the cortical actin network is important for the coupling of retraction to protrusion. Previous work has shown that retraction at the rear of a cell can passively follow as a result of trailing from tension generated by protrusion (Chen, 1981; Oliver et al., 1994). In addition, retraction can be actively promoted by myosin II-mediated contraction (Egelhoff and Spudich, 1991; Jay et al., 1994). Since the activity of myosin II is regulated by phosphorylation of its heavy and light chains, it is plausible to assume that myosin II kinases or phosphatases are regulated in response to signals that are propagated from the front to the rear. A mechano-chemical mode of signal transmission might be envisaged for the regulation of myosin activities. For example, the myosin phosphorylation machinery could be sensitive to cortical tension.

The actin system also plays a role in coordinating the gain and loss of contact area, a function that is supported by appropriate adhesion of the cells to a substratum (Fig. 8D versus L, and J, and N versus L and P). The strong tendency in wild-type cells for loss to follow gain indicates that contact formation is the leading event (Fig. 8A and C), and that a signal emanates from this event that causes detachment at regions behind the new area of contact (Fig. 8B and D). These results are in line with findings on cell-to-substratum interactions in fibroblasts. Adhesive structures couple to the cytoskeleton in mouse 3T3 cells while the contact area grows in size (Schmidt et al., 1993; Sheetz, 1994). The cytoskeleton provides a rearward traction force to an attached membrane area which allows the cell body to move forward. The detaching region of the rear is distinguished from the attaching front by a stronger deformability of the membrane (Schmidt et al., 1993). Integrin-cytoskeleton interaction is reduced at the rear, which leads to weakened cell-substratum interaction and thus facilitates detachment.

Experiments and theoretical considerations of Gingell and co-workers have focused attention onto adhesion-sensitive signalling mechanisms in *Dictyostelium* cells (Gingell and Vince, 1982; Owens et al., 1988; Gingell and Owens, 1992). Upon attachment to a surface, a contractile response is induced that causes the rear portion of the cell to spread into a thin lamella. This response is myosin II dependent (Jay et al., 1994). The chemical nature of the surface is not critical for this response; only its strong adhesiveness is relevant. These results have been interpreted in terms of a function of the membrane as a contact transducer (Gingell and Owens, 1992). Adhesive trapping of proteins diffusing in the plane of the membrane is thought to induce a response at the cytoplasmic face of the membrane. Clustering of the entrapped membrane proteins may elicit production of secondary messengers like cGMP, $IP_3$ or diacylglycerol, that influence the assembly of cytoskeletal proteins (Schleicher and Noegel, 1992; Janmey, 1994). Alternatively, clustered proteins may directly affect actin polymerisation or myosin I association with the membrane (Cooper, 1991; Pollard et al., 1991). Two membrane-bound proteins of *D. discoideum*, hisactophilin and ponticulin, are in fact known to nucleate actin polymerisation (Scheel et al., 1989; Hitt et al., 1994).

The results reported in this paper and in a previous one (Schindl et al., 1995) on TP1 and other mutants defective in three actin-binding proteins, markedly differ from those obtained with mutants lacking myosin II. A characteristic of myosin II null cells is their deficiency in rounding up and detaching from a surface under conditions of ATP depletion (Pasternak et al., 1989). In contrast, TP1 cells have difficulty in attaching. The results obtained with TP1 and myosin II null mutants can be rationalised by assuming that the myosin produces rigor that tends to round up the cell, whereas the actin-binding proteins missing in TP1 counterbalance that rigor. Myosin II null cells have to cope with their inefficient production of rigor required for detachment from a substratum by contraction. Therefore, phenotypic changes observed in myosin II null cells are most pronounced on a strongly adhesive surface such as polylysine-coated glass (Jay et al., 1994). In contrast, the actin-binding proteins eliminated by mutation provide the cell cortex with the mechanical properties that enable a cell to attach and spread over an area of finite size. On a weakly adhesive surface like mica, where a cell relies for control of its locomotion on the optimal function of its cytoskeleton, aberrations in the mutants are most obvious. On a more strongly adhesive surface, e.g. albumin-coated glass, the forces of adhesion compensate for a loss in stability of the actin cortex, so that the cells can stabilise their motion even in the absence of α-actinin, the 120 kDa gelation factor, and severin.

We are indebted to Erich Sackmann, Mathias Schindl and Elliot Elson for helpful discussions. This work was supported by the Deutsche Forschungsgemeinschaft (SFB 266/D7). I. W. received a PhD grant from the Max Planck Society.

## REFERENCES

**Albrecht-Bühler, G.** (1990). In defense of 'nonmolecular' cell biology. *Int. Rev. Cytol.* **120**, 191-241.

**Alt, W.** (1990a). Correlation analysis of two-dimensional locomotion paths. In *Biological Motion*. Springer Series: *Lecture Notes in Biomathematics*, vol. 89 (ed. W. Alt and G. Hoffmann), pp. 254-268. Berlin: Springer Verlag.

**Alt, W.** (1990b). Mathematical models and analysing methods for the lamellipodial activity of leukocytes. In *Biomechanics of Active Movement*

*and Deformation of Cells*, NATO ASI Series H42 (ed. N. Akkas), pp. 403-422. Berlin: Springer Verlag.

**André, E., Brink, M., Gerisch, G., Isenberg, G., Noegel, A., Schleicher, M., Segall, J. E. and Wallraff, E.** (1989). A *Dictyostelium* mutant deficient in severin, an F-actin fragmenting protein, shows normal motility and chemotaxis. *J. Cell Biol.* **108**, 985-995.

**Brink, M., Gerisch, G., Isenberg, G., Noegel, A. A., Segall, J. E., Wallraff, E. and Schleicher, M.** (1990). A *Dictyostelium* mutant lacking an F-actin cross-linking protein, the 120-kD gelation factor. *J. Cell Biol.* **111**, 1477-1489.

**Brown, S. S., Yamamoto, K. and Spudich, J. A.** (1982). A 40,000-dalton protein from *Dictyostelium discoideum* affects assembly properties of actin in a $Ca^{2+}$-dependent manner. *J. Cell Biol.* **93**, 205-210.

**Chen, W.-T.** (1981). Mechanism of retraction of the trailing edge during fibroblast movement. *J. Cell Biol.* **90**, 187-200.

**Condeelis, J., Vahey, M., Carboni, J. M., DeMey, J. and Ogihara, S.** (1984). Properties of the 120,000- and 95,000-dalton actin-binding proteins from *Dictyostelium discoideum* and their possible functions in assembling the cytoplasmic matrix. *J. Cell Biol.* **99**, 119s-126s.

**Condeelis, J.** (1993). Understanding the cortex of crawling cells: insights from *Dictyostelium*. *Trends Cell Biol.* **3**, 371-376.

**Cooper, J. A.** (1991). The role of actin polymerization in cell motility. *Annu. Rev. Physiol.* **53**, 585-605.

**Cox, D., Condeelis, J., Wessels, D., Soll, D., Kern, H. and Knecht, D. A.** (1992). Targeted disruption of the ABP-120 gene leads to cells with altered motility. *J. Cell Biol.* **116**, 943-955.

**Curtis, A. S. G.** (1964). The mechanism of adhesion of cells to glass. A study by interference reflection microscopy. *J. Cell Biol.* **20**, 199-215.

**Dickinson, R. B. and Tranquillo, R. T.** (1993). A stochastic model for adhesion-mediated cell random motility and haptotaxis. *J. Math. Biol.* **31**, 563-600.

**DiMilla, P. A., Barbee, K. and Lauffenburger, D. A.** (1991). Mathematical model for the effects of adhesion and mechanics on cell migration speed. *Biophys. J.* **60**, 15-37.

**DiMilla, P. A., Stone, J. A., Quinn, J. A., Albelda, S. M. and Lauffenburger, D. A.** (1993). Maximal migration of human smooth muscle cells on fibronectin and type IV collagen occurs at an intermediate attachment strength. *J. Cell Biol.* **122**, 729-737.

**Dunn, G. A.** (1983). Characterising a kinesis response: Time avaraged measures of cell speed and directional persistence. *Agents and Actions Suppl.* **12**, 14-33.

**Dunn, G. A. and Brown, A. F.** (1986). Alignment of fibroblasts on grooved surfaces described by a simple geometric transformation. *J. Cell Sci.* **83**, 313-340.

**Dunn, G. A. and Brown, A. F.** (1987). A unified approach to analysing cell motility. *J. Cell Sci. Suppl.* **8**, 81-102.

**Egelhoff, T. T. and Spudich, J. A.** (1991). Molecular genetics of cell migration: *Dictyostelium* as a model system. *Trends Genetics* **7**, 161-166.

**Eichinger, L. and Schleicher, M.** (1992). Characterization of actin- and lipid-binding domains in severin, a $Ca^{2+}$-dependent F-actin fragmenting protein. *Biochemistry* **31**, 4779-4787.

**Fisher, P. R., Merkl, R. and Gerisch, G.** (1989). Quantitative analysis of cell motility and chemotaxis in *Dictyostelium discoideum* by using an image processing system and a novel chemotaxis chamber providing stationary chemical gradients. *J. Cell Biol.* **108**, 973-984.

**Galbraith, W. and Farkas, D. L.** (1993). Remapping disparate images for coincidence. *J. Microsc.* **172**, 163-176.

**Gerisch, G., Hülser, D., Malchow, D. and Wick, U.** (1975). Cell communication by periodic cyclic-AMP pulses. *Phil. Trans. R. Soc. Lond.* B **272**, 181-192.

**Gerisch, G. and Keller, H. U.** (1981). Chemotactic reorientation of granulocytes stimulated with micropipettes containing *fMet-Leu-Phe*. *J. Cell Sci.* **52**, 1-10.

**Gerisch, G., Albrecht, R., de Hostos, E., Wallraff, E., Heizer, C., Kreitmeier, M. and Müller-Taubenberger, A.** (1993). Actin-associated proteins in motility and chemotaxis of *Dictyostelium* cells. In *Cell Behaviour: Adhesion and Motility*, Symposia of the Society for Experimental Biology, vol. 47 (ed. G. Jones, C. Wigley and R. Warn), pp. 297-315. Cambridge: The Company of Biologists.

**Gingell, D. and Todd, I.** (1979). Interference reflection microscopy. A quantitative theory for image interpretation and its application to cell-substratum separation measurement. *Biophys. J.* **26**, 507-526.

**Gingell, D. and Vince, S.** (1982). Substratum wettability and charge influence the spreading of *Dictyostelium* amoebae and the formation of ultrathin cytoplasmic lamellae. *J. Cell Sci.* **54**, 255-285.

**Gingell, D., Todd, I. and Owens, N.** (1982). Interaction between intracellular vacuoles and the cell surface analysed by finite aperture theory interference reflection microscopy. *J. Cell Sci.* **54**, 287-298.

**Gingell, D. and Owens, N.** (1992). How do cells sense and respond to adhesive contacts? Diffusion-trapping of laterally mobile membrane proteins at maturing adhesions may initiate signals leading to local cytoskeletal assembly response and lamella formation. *J. Cell Sci.* **101**, 255-266.

**Grebecki, A. (**1994). Membrane and cytoskeleton flow in motile cells with emphasis on the contribution of free-living amoebae. *Int. Rev. Cytol.* **148**, 37-80.

**Harris, A. K.** (1994). Locomotion of tissue culture cells considered in relation to ameboid locomotion. *Int. Rev. Cytol.* **150**, 35-68.

**Hitt, A. L., Hartwig, J. H. and Luna, E. J.** (1994). Ponticulin is the major high affinity link between the plasma membrane and the cortical actin network in *Dictyostelium*. *J. Cell Biol.* **126**, 1433-1444.

**Janmey, P. A.** (1994). Phosphoinositides and calcium as regulators of cellular actin assembly and disassembly. *Annu. Rev. Physiol.* **56**, 169-191.

**Jay, P. Y., Pasternak, C. and Elson, E. L.** (1994). A role of myosin-II in the locomotion of *Dictyostelium* amoebae. *J. Cell. Biochem. Suppl.* **18C**, 243-243.

**Killich, T., Plath, P. J., Wei, X., Bultmann, H., Rensing, L. and Vicker, M. G.** (1993). The locomotion, shape and pseudopodial dynamics of unstimulated *Dictyostelium* cells are not random. *J. Cell Sci.* **106**, 1005-1013.

**Lauffenburger, D. A.** (1989). A simple model for the effects of receptor-mediated cell-substratum adhesion on cell migration. *Chem. Eng. Sci.* **44**, 1903-1914.

**Lee, J., Ishihara, A., Theriot, J. A. and Jacobson, K.** (1993). Principles of locomotion for simple-shaped cells. *Nature* **362**, 167-171.

**Luna, E. J. and Condeelis, J. S.** (1990). Actin-associated proteins in *Dictyostelium discoideum*. *Dev. Genet.* **11**, 328-332.

**Malchow, D., Nägele, B., Schwarz, H. and Gerisch, G.** (1972). Membrane-bound cyclic AMP phosphodiesterase in chemotactically responding cells of *Dictyostelium discoideum*. *Eur. J. Biochem.* **28**, 136-142.

**Oliver, T., Lee, J. and Jacobson, K.** (1994). Forces exerted by locomoting cells. *Semin. Cell Biol.* **5**, 139-148.

**Owens, N. F., Gingell, D. and Bailey, J.** (1988). Contact-mediated triggering of lamella formation by *Dictyostelium* amoebae on solid surfaces. *J. Cell Sci.* **91**, 367-377.

**Pasternak, C., Spudich, J. A. and Elson, E. L.** (1989). Capping of surface receptors and concomitant cortical tension are generated by conventional myosin. *Nature* **341**, 549-551.

**Pollard, T. D., Doberstein, S. K. and Zot, H. G.** (1991). Myosin I. *Annu. Rev. Physiol.* **53**, 653-681.

**Rädler, J. and Sackmann, E.** (1993). Imaging optical thicknesses and separation distances of phospholipid vesicles at solid surfaces. *J. Phys. II France* **3**, 727-748.

**Russ, J. C.** (1990). *Computer-assisted Microscopy: The Measurement and Analysis of Images.* New York, London: Plenum Press.

**Sackmann, E.** (1994). Intra- and extracellular macromolecular networks: Physics and biological function. *Macromol. Chem. Phys.* **195**, 7-28.

**Scheel, J., Ziegelbauer, K., Kupke, T., Humbel, B. M., Noegel, A. A., Gerisch, G. and Schleicher, M.** (1989). Hisactophilin, a histidine-rich actin-binding protein from *Dictyostelium discoideum*. *J. Biol. Chem.* **264**, 2832-2839.

**Schindl, M., Wallraff, E., Deubzer, B., Witke, W., Gerisch, G. and Sackmann, E.** (1995). Cell-substrate interactions and locomotion of *Dictyostelium* wild-type and mutants defective in three cytoskeletal proteins: A study using quantitative reflection interference contrast microscopy. *Biophys. J.* (in press).

**Schleicher, M. and Noegel, A. A.** (1992). Dynamics of the *Dictyostelium* cytoskeleton during chemotaxis. *New Biol.* **4**, 461-472.

**Schmidt, C. E., Horwitz, A. F., Lauffenburger, D. A. and Sheetz, M. P.** (1993). Integrin-cytoskeletal interactions in migrating fibroblasts are dynamic, asymmetric, and regulated. *J. Cell Biol.* **123**, 977-991.

**Sheetz, M. P., Wayne, D. B. and Pearlman, A. L.** (1992). Extension of filopodia by motor-dependent actin assembly. *Cell Motil. Cytoskel.* **22**, 160-169.

**Sheetz, M. P.** (1994). Cell migration by graded attachment to substrates and contraction. *Semin. Cell Biol.* **5**, 149-155.

**Simon, S. I. and Schmid-Schönbein, G. W.** (1990). Cytoplasmic strains and strain rates in motile polymorphonuclear leukocytes. *Biophys. J.* **58**, 319-332.

**Soll, D. R.** (1988). 'DMS', a computer-assisted system for quantitating motility, the dynamics of cytoplasmic flow and pseudopod formation: its application to *Dictyostelium* chemotaxis. *Cell Motil. Cytoskel.* **10**, 91-106.

**Stokes, C. L., Lauffenburger, D. A. and Williams, S. K.** (1991). Migration of individual microvessel endothelial cells: Stochastic model and parameter measurement. *J. Cell Sci.* **99**, 419-430.

**Titus, M. A.** (1993). Myosins. *Curr. Opin. Cell Biol.* **5**, 77-81.

**Verschueren, H.** (1985). Interference reflection microscopy in cell biology: methodology and applications. *J. Cell Sci.* **75**, 279-301.

**Wallraff, E., Schleicher, M., Modersitzki, M., Rieger, D., Isenberg, G. and Gerisch, G.** (1986). Selection of *Dictyostelium* mutants defective in cytoskeletal proteins: Use of an antibody that binds to the ends of α-actinin rods. *EMBO J.* **5**, 61-67.

**Wessels, D., Vawter-Hugart, H., Murray, J. and Soll, D. R.** (1994). Three-dimensional dynamics of pseudopod formation and the regulation of turning during the motility cycle of *Dictyostelium*. *Cell Motil. Cytoskel.* **27**, 1-12.

**Witke, W., Schleicher, M. and Noegel, A. A.** (1992). Redundancy in the microfilament system: Abnormal development of *Dictyostelium* cells lacking two F-actin cross-linking proteins. *Cell* **68**, 53-62.

**Witke, W., Hofmann, A., Köppel, B., Schleicher, M. and Noegel, A. A.** (1993). The $Ca^{2+}$-binding domains in non-muscle type α-actinin: Biochemical and genetic analysis. *J. Cell Biol.* **121**, 599-606.

(Received 25 November 1994 - Accepted 16 January 1995)